CDF Run-II silicon detector: operations and aging

Michelle STANCARI[*][†]

Fermi National Accelerator Laboratory

E-mail: `mstancar@fnal.gov`

The CDF Run-II silicon microstrip detector has seen almost 12 fb^{-1} of proton-antiproton collisions over the last 10 years. It has shown remarkable performance, with 80% of its channels still operating error-free, and only one of its eight layers approaching the operational limits for full depletion. The measured depletion voltage and signal-to-noise ratio of these sensors give unique information about the behavior of sensors irradiated slowly over a long period of time. Data from heavily irradiated, double-sided sensors excludes a monotonic electric field inside the sensor and is instead consistent with a doubly-peaked field that is lower in the center of the sensor and higher at the edges.

---

[*]Speaker.

[†]for the CDF Run-II Silicon Group
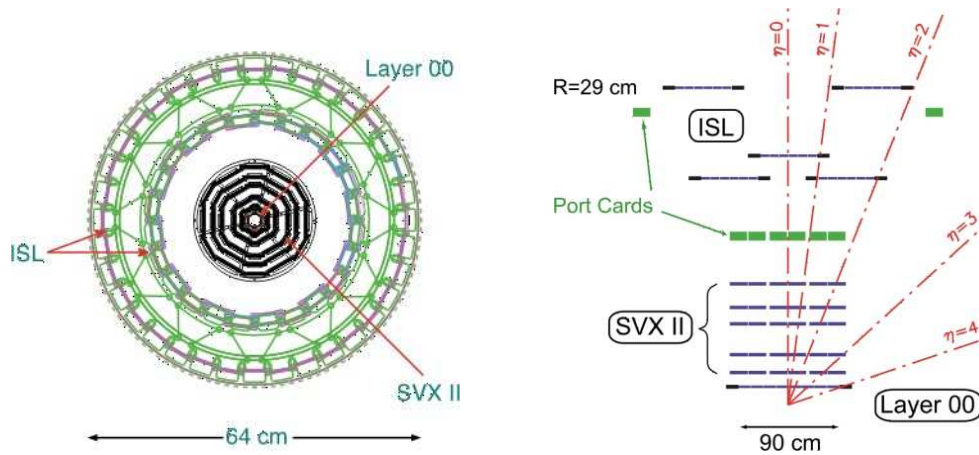
Figure 1: A schematic layout of the three subdetectors.

1. Introduction

The Tevatron at Fermi National Accelerator Laboratory collides proton and antiproton beams at a center-of-mass energy of 1.96 TeV. These collisions are observed by two multi-purpose detectors, CDF and DØ. The broad Tevatron Run-II physics program includes precision electroweak measurements (top and W boson masses), bottom and charm physics, the Higgs boson, and searches for physics beyond the standard model.

Combined with other tracking detectors, the primary purpose of the Run-II silicon detectors is identification of displaced secondary vertices. These were the largest HEP silicon detectors of their generation, and the first with dynamic pedestal subtraction and deadtimeless operation. CDF's Silicon Vertex Tracker performs high precision tracking in time for a L2 decision, by means of a pattern recognition technique, exploiting silicon hits and tracks reconstructed in the outer tracking detector. Offline-like precision is achieved on track parameters, allowing to effectively trigger on tracks displaced from the primary vertex[1].

The Tevatron silicon detectors were designed to withstand 2-3 fb^{-1} of integrated luminosity and then be replaced in 2004. These upgrades were canceled and Run-II was eventually extended through 2011. Consequently, the original detectors have been exposed to 4-5 times the anticipated radiation dose. The remarkable performance of these sensors under long term exposure provides unique and relevant data about radiation damage in silicon detectors. The Tevatron also offers operational perspective and practical experience that is invaluable to current and future experiments that rely on silicon tracking detectors.

2. Detector Description

The CDF Run-II silicon detector system consists of three sub-detector: Layer 00 (L00), the Silicon VerteX detector (SVX) and the Intermediate Silicon Layers (ISL). The schematic layout of the system is shown in Fig. 1 and table 1 lists some characteristic parameters. The elemental unit of a sub-detector is a ladder, which consists of multiple silicon sensors that share common communication lines and power connections. SVX and ISL are composed of double-sided microstrip

Name	Radius (cm)	Readout	Manufacturer
L00 (narrow)	1.35	$r\phi$	SGS Thomson, Micron
L00 (wide)	1.62	$r\phi$	Hamamatsu
SVX L0	2.54	$r\phi$,z	Hamamatsu
SVX L1	4.12	$r\phi$,z	Hamamatsu
SVX L2	6.52	$r\phi$,$1.2°$	Micron
SVX L3	8.22	$r\phi$,z	Hamamatsu
SVX L4	10.10	$r\phi$,$1.2°$	Micron
ISL L6 Central	22.00	$r\phi$,$1.2°$	Hamamatsu
ISL L6 Fwd/Bwd	20.00	$r\phi$,$1.2°$	Hamamatsu
ISL L7 Fwd/Bwd	28.00	$r\phi$,$1.2°$	Micron

Table 1: Summary of some basic paramters for L00, SVX and ISL. The readout column specifies the orientation of the microstrips in the cylindrical coordinate system of the detector. On the double sided sensors, the second face of strips is either oriented $90°$ with respect to the first set ($r\phi$,z) or at a small stereo angle ($r\phi$,$1.2°$). The strips that measure the $r\phi$ coordinate are always on the p-side of the sensor.

sensors, while L00 has single-sided microstrip sensors. In all cases, the sensors are standard p-in-n style. For the CDF double sided sensors, the p-side is often called the *phi-side* because it measures the ϕ coordinate and the n-side called the *z-side*. A small fraction of the L00 sensors were made with oxygenated silicon to evaluate its radiation hardness.

SVX was designed for optimal displaced vertex detection, and and tracking. ISL was added to increase the η coverage of silicon tracks and L00 was added to compensate the eventual loss of the innermost layer of SVX (layer 0) to radiation damage and improve the impact parameter resolution. The expected lifetime of the L00 sensors is longer than the SVX sensors, despite the increased radiation dose closer to the beampipe. The sensors must be both fully depleted and sensitive (S/N>6) for the data to be useful, and both issues must be addressed to improve detector lifetime.

The L00 sensors can withstand up to 650 V in bias voltage, while the SVX sensors breakdown around 200 V. The weak point is the decoupling capacitors, which can handle $\sim$100 V. Double-sided sensors have one capacitor on each side, so these capacitors limit the bias voltage the can be applied. Single sided sensors, with only one capacitor which can be strategically grounded, are not limited by the capacitor's breakdown voltage.

The L00 sensors are actively cooled to approximately -5$°$C on separate cooling lines from the readout chips, roughly 10-15$°$C colder than the SVX sensors. This reduces the sensor leakage current and its contribution to the overall noise. In addition, the L00 readout chips are located outside the tracking volume, thus noise growth in the chips due to radiation damage is reduced compared with SVX.

3. Performance

A variety of unexpected causes of ladder and/or readout chip failures appeared at the beginning
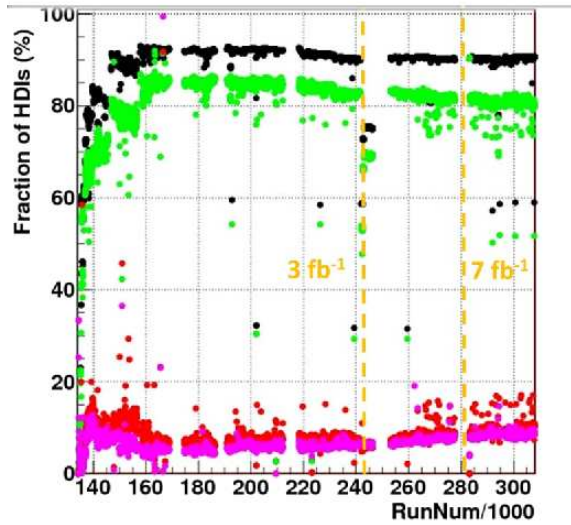
Figure 2: The fraction of ladders considered good (green) and bad (red) vs run number. The fraction of ladders integrated into data taking is shown in black and the average digital error rate in pink. A ladder is considered good if it has a digital error rate smaller than 1%. Note that the run numbers do not scale linearly with luminosity. Instead, dashed lines are drawn to provide a couple reference points.

of Run-II. These include beam incidents, wire bond resonances, and thermal cycles, and are well-documented elsewhere[2]. After commissioning, which included additional protection systems to prevent further damage, 85% of ladders were operating without errors. After 10 years, 80% of all ladders are still operating without digital errors, as shown by the green points in Fig. 2. The failure rate of $\sim$0.5% of ladders per year[1], is constant with time after commisioning and dominated by chip failures. The symptoms of the chip failures range in severity from bit errors local to the chip to communication failure that blocks the data bus for the entire ladder. The specific failure within the chip as well as the external cause (radiation, age, thermal cycles) are not understood. In addition to the chip failures, a few ladders have developed errors due to failure of optical data transmitters[3] unaccessable for repair.

4. Aging

Radiation damage affects the sensors in two principle ways: the increase of bias voltage required to deplete the sensor and the decrease of signal-to-noise ratio. CDF monitors both quantities, raising the bias voltage settings as needed to maximize charge collection.

4.1 Signal to Noise Ratio

The signal-to-noise ratio (S/N) is monitored continuously with tracks in events acquired with muon triggers for study of J/ψ decays in physics analyses. The signal is the total cluster charge only for muon tracks, corrected for path length in the sensor. The noise for each individual strip

---

[1]This is equivalent to $\sim$0.05% of the chips per year. The number of chips per ladder increases from 3 to 16 with radius as the number of strips per sensor increases, 8 chips per ladder on average, and 4248 chips in total.
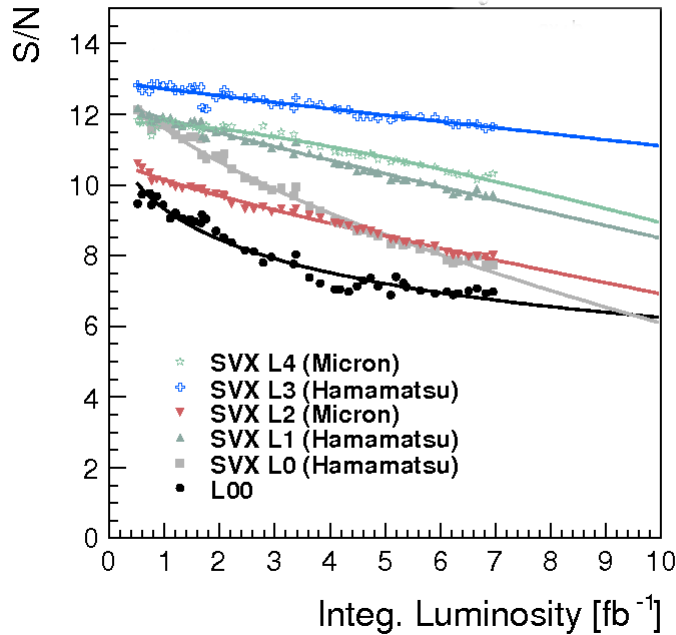
Figure 3: The average S/N ratio for the phi-side of the SVX ladders and L00. The points are fit to the function $y = \frac{Ax+B}{C\sqrt{x}+D}$. The extrapolations are valid only while the sensors are fully depleted.

is measured regularly with special runs with colliding beams at low instantaneous luminosity. The noise for a muon hit is the average of the noise of the strips participating in the cluster.

The measured S/N ratio for SVX and L00 are shown in Fig. 3. The decrease with luminosity is fit to an empirical formula that combines the expected noise growth with a linear signal decrease, and these fits are used to predict the future detector performance. For S/N below 6, the performance of that sensor is affected. Layer 0 of SVX is the only layer expected to reach this value before the end of the run, about the time that the depletion voltage reaches the sensor breakdown value. However, internal studies indicate that the ability of CDF to identify b-hadron decays by detecting a displaced secondary vertex (b-tagging) is not compromised by the loss of layer 0.

Additional information is contained in the separate S and N values, shown in Fig. 4 for L00 and layer 0 of SVX. Due to its proximity to the beampipe, L00 is subject to twice the radiation dose that SVX layer 0 receives for the same number of collisions and the reduced noise in L00 is necessary for its extended lifetime. It is not known at this time the key factor in the reduced noise, but the colder operating temperature and the shielding of the readout chips are two possible contributors. The strange flattening of the signal in L00 after 4 fb^{-1} not yet understood.

4.2 Depletion Voltage

The depletion voltage of the sensors is monitored by measuring the charge collected for tracks traversing the sensor as a function of bias voltage. This requires dedicated running with colliding beams, and is done at the expense of physics data. The tracks are defined by CDF's central outer
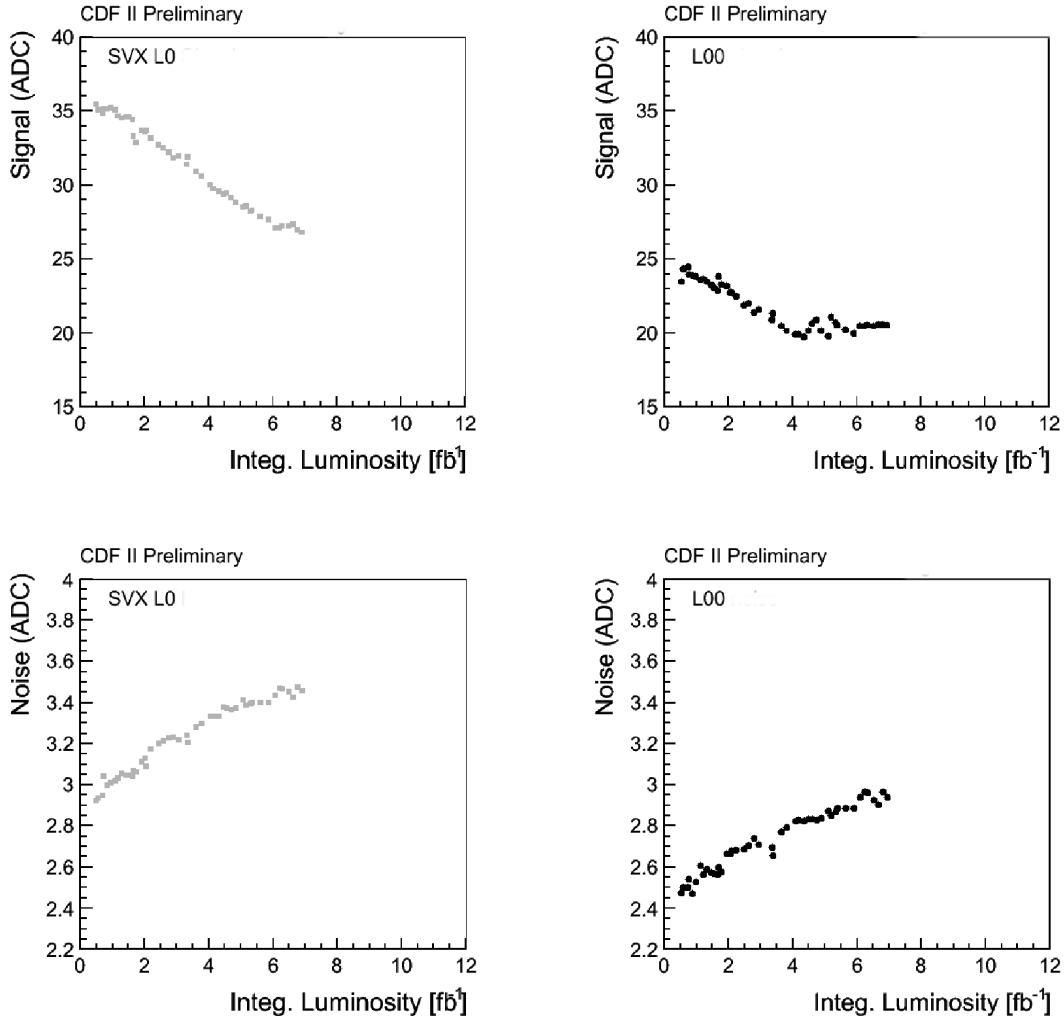
Figure 4: The evolution of the signal and the noise used to calculate S/N.

tracker and the remaining silicon layers, and then a cluster is searched for in the layer under study within 150 μm of the track.

The charge of each found cluster is histogrammed, and for each bias voltage, the peak of this histogram is determined by fitting the region around the peak to the convolution of a Landau and a Gaussian function. The upper two plots of Fig. 5 are example histograms and their fits for a L00-narrow ladder at a bias voltage of 30 V (left) and 130 V (right). For each bias voltage setting, the most probable cluster charge and the efficiency are determined, and the lower left plot of Fig. 5 shows the results for a scan taken at 4 fb^{-1} of integrated luminosity.

The lower left plot of Fig. 5 summarizes much about the sensor in a single plot, and is useful operationally to evaluate the status of the detector visually comparing ladders in the same layer. The value at which the cluster charge saturates should and does agree with the *signal* from J/ψ muons calculated for the S/N studies even though the track selections and reconstructions differ. The cluster charge for small voltages reveals the effective clustering threshold of the standard of-
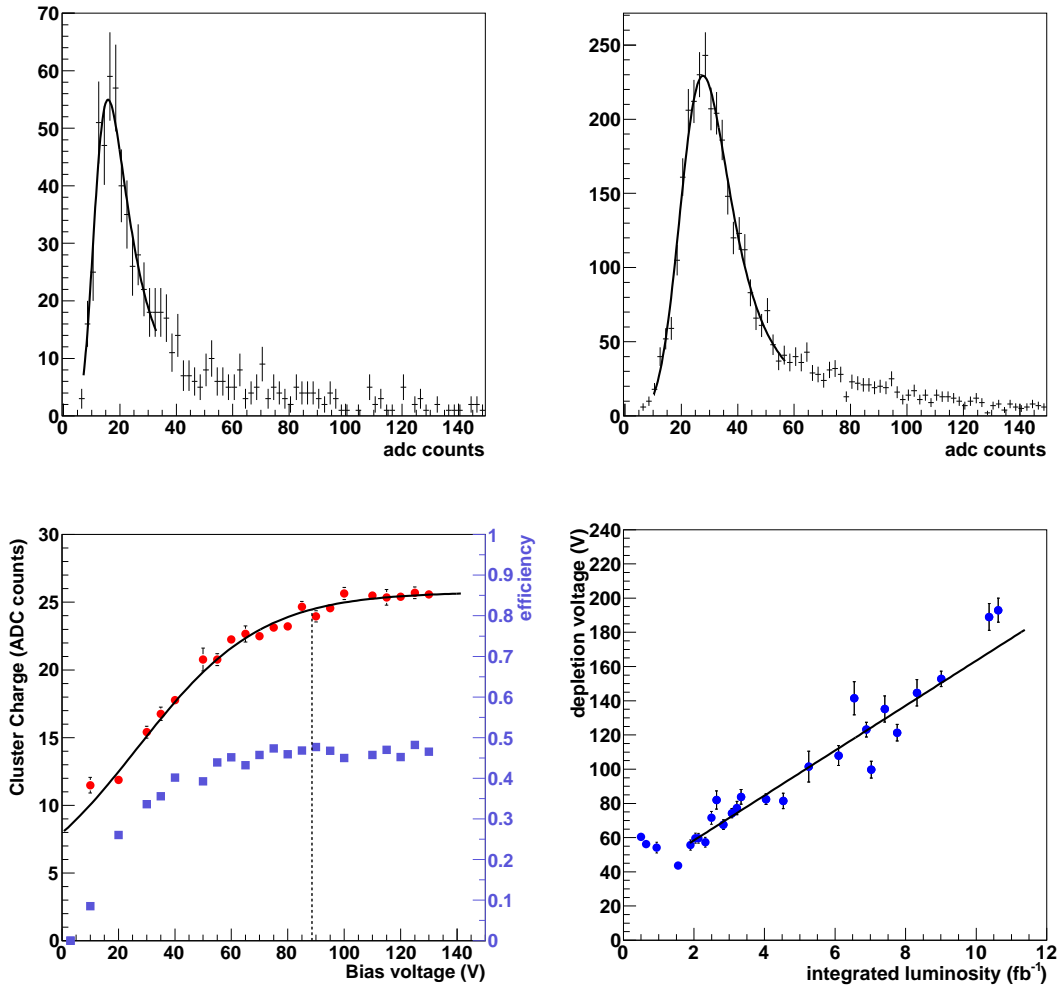
Figure 5: The upper plots show the measured cluster charge distribution for a single L00-narrow ladder (LB0W1L3) at a bias voltage of 30 V (left) and 130 V (right) after 4 fb^{-1} of luminosity. The lower left plot shows the peak of the cluster charge distribution (red circles) as a function of bias voltage. The dashed line indicates the depletion voltage extracted from the sigmoid fit. The lower right plot is the measured depletion voltage for this ladder as a function of integrated luminosity, and the linear fit used to extrapolate to higher luminosity values.

fline analysis for that sensor, convoluted with the pedestal cut of the zero-suppressed readout. The clustering thresholds are derived run-by-run from the measured noise in each individual strip. Radiation damage gradually increases the noise, and clustering thresholds need to be monitored.

The efficiency shown on this plot is defined as the fraction of tracks for which a cluster is found within 150 μm of the track path. Tracks with more than one cluster in this region are discarded. The track selection is quite loose due to limited statistics of special data runs, so the value at which the efficiency saturates is not a relevant quantity for sensor performance. The sensor performance can instead be evaluated from the Jψ muon tracks used for the S/N studies, but these results are not yet available.
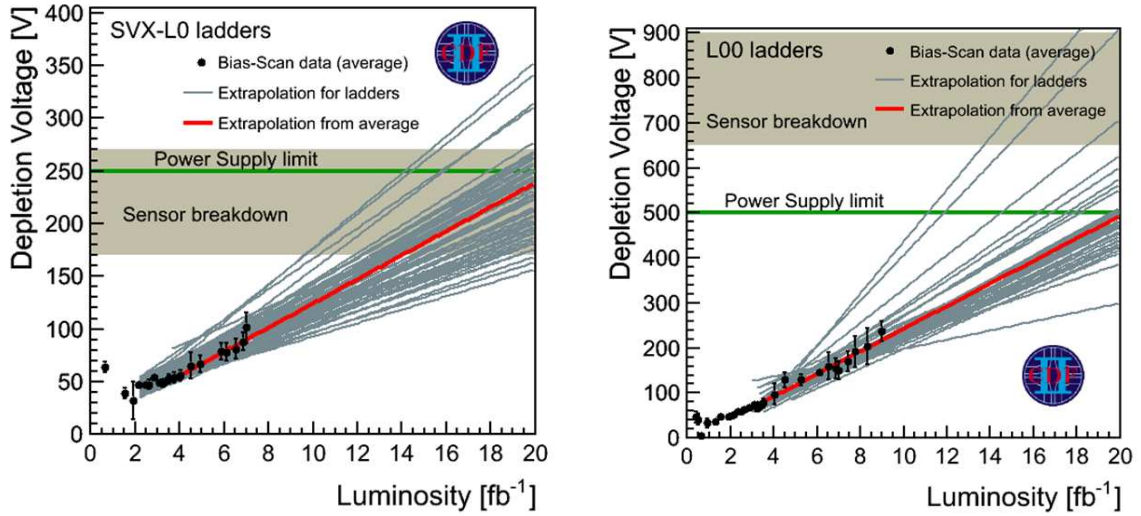
Figure 6: The measured depletion voltage, averaged over all ladders is shown as black points for layer 0 of SVX (SVX-L0) on the left and L00 on the right. The lines shown the extrapolations to higher luminosity for the individual ladders.

The measured cluster charge as a function of bias voltage shown in the lower right plot of Fig. 5, is fit to a sigmoid function whose lower limit is allowed to be different than zero to accomodate the clustering threshold. The measured depletion voltage is defined as the voltage at which the cluster charge reaches 95% of its saturation value. The depletion voltages measured at different luminosities are shown in the lower right plot. The points well after type inversion are fit to a straight line, and the extrapolation of this line is used when deciding how much to increase the operating voltage.

The best fit lines for all the sensors in layer 0 of SVX and L00 and the average depletion voltage are shown in Fig. 6. The range of breakdown voltages for test sensors is shown as a shaded region in the plots while the maximum voltage that the power supplies can provide is shown as a horizontal line. These are two limitations on the operating voltage. The spread in the slope of the lines for L00 is enhanced by the fact that the difference in radiation dose for individual sensors due to changing beam positions is not negligible with the layer being this close to the interaction region.

Different layers can be compared by converting integrated luminosity to radiation dose using the radiation field inside the CDF detector measured with TLDs in 2001[4] and assuming that the interaction region is in the center of the detector. Fig. 7 compares the measured depletion voltage, averaged over all identical ladders, for different categories of sensors in L00 with layer 0 of SVX. The L00 narrows are closer to the interaction region than the L00 wides, but only the oxygenated narrow ladders are expected to have a different response to radiation.

While there is a distinct difference in S/N behavior for L00 and layer 0 of SVX, attributable in large part to the colder operating temperature of L00, after inversion the depletion voltages behave the same as expected. A difference in slope for the oxygenated sensors is expected, and further data analysis, with an accurate calculation of the radiation dose from the measured beam
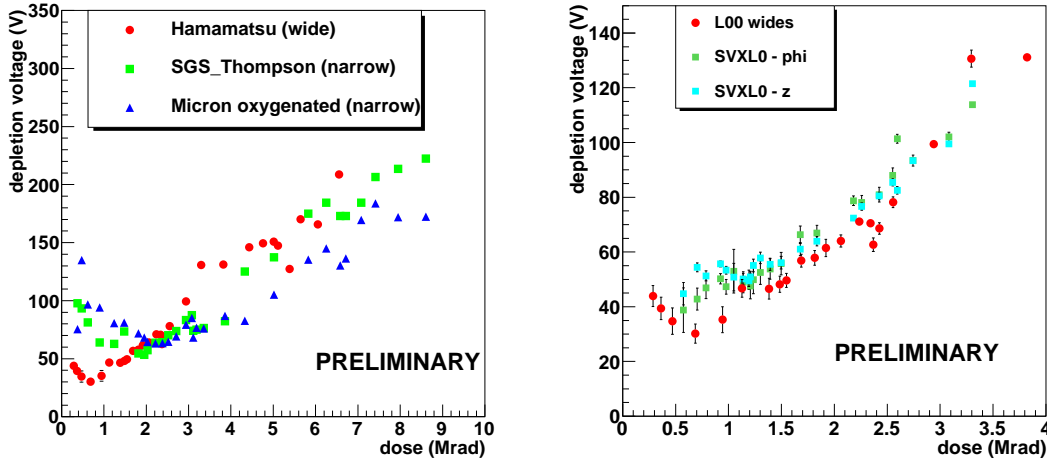
Figure 7: A comparison of the measured depletion voltages for different silicon layers. The L00 sensors are shown on the left, separated by sensor type, On the right, the wide L00 sensors are compared with the innermost layer of SVX.
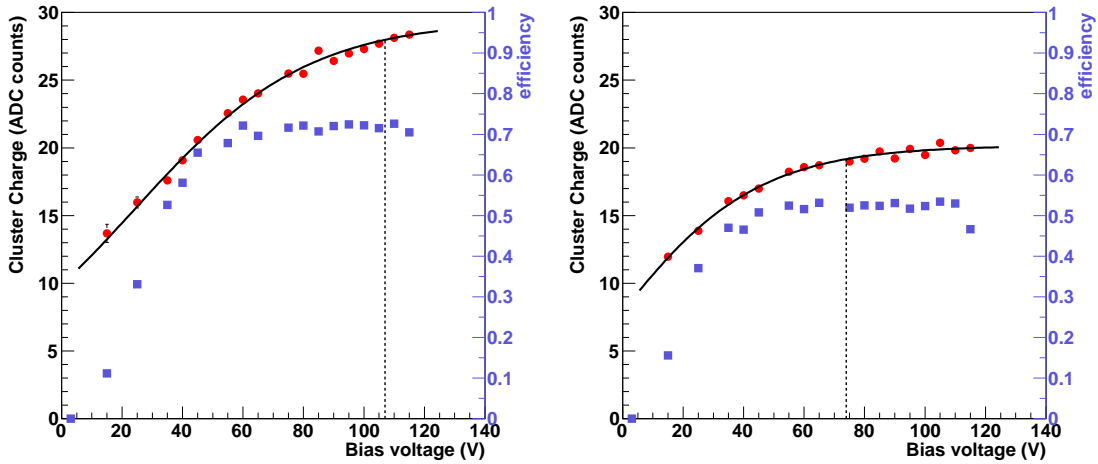
Figure 8: The cluster charge as a function of bias voltage for the p-side (left) and n-side (right) of a SVX layer 0 sensor. These data were taken after 6.9 fb^{-1} of delivered luminosity, and the sensor inverted after roughly 1.5 fb^{-1}.

position, is needed to quantify this difference. To compare these results with other studies of radiation damage, a conversion to 1 MeV neutron equivalents can be estimated. Assuming that the contribution of photons and low energy neutrons to the TLD measurements is negligible, that the MIPs are predominantly pions, and that these pions do half the damage of a 1 MeV neutron, one obtains the conversion 1 Mrad $\sim 3.87 \times 10^{13}$ MIPs $\sim 2 \times 10^{13}$ 1 MeV neutrons.

4.3 Evidence for Double-Peaked Electric Fields and Operational Consequences

It is well known that the electric field inside a depleted silicon sensor varies linearly as a function of depth before irradiation. Recently, it has been demonstrated that heavily irradiated sensors behave differently, and the internal electric field exhibits maxima near the electrodes at either edge of the sensor.[5] Fig. 8 shows the measured charge collected as a function of bias voltage for both sides of a typical sensor from layer 0 of SVX. These data are inconsistent with a monotonic electric field inside the sensor and instead suggest an electric field with two peaks, one at each edge of the sensor. In addition, a linear electric field after type inversion should produce a steep turn on near the depletion voltage for the p-side of the L00 sensors, and this is not the case as seen in the lower left plot of Fig. 5.

This unexpected (at the time of the detector design) electric field behavior has an important consequence for the longevity of the CDF silicon detector. According to the projections in Fig. 6, several of the layer 0 ladders will not be fully depleted at the end of Run-II if the bias voltage is not raised above 170 V, where sensor breakdown is believed to start. If, when slightly underdepleted, one side of the the double-sided sensor would no longer have a signal, and the risk of raising the voltages is justified. However, Fig. 8 shows that both sides of the sensor will to continue to provide hit information for some limited period of time despite being slightly underdepleted, and the risk of raising the voltages beyond 170 V was not worth the small potential gain for a handful of sensors during the last 6 months of the Run-II.

5. Conclusions

The Run-II CDF silicon detector is performing extremely well after 10 years of experimental running. Studies of radiation damage reveal important information about detector longevity in an experimental environment. The doubly-peaked electric field inside the heavily irradiated sensors, and the resulting charge collection behavior as a function of bias voltage, were different than expected when the detector was designed, and this difference affected operational decisions during the last year of the run.

References

[1] J. Adelman, et al., Nucl. Instrum. Meth. A **572** (2007) 361.

[2] G. Bolla, et al., Nucl. Instrum. Meth. A **518** (2004) 277.
    C. Hill, et al., Nucl. Instrum. Methods A **511** (2003) 118.

[3] S. Hou, et al., Nucl. Instrum. Meth. A **511** (2003) 166.

[4] R. J. Tesarek, et al., Nucl. Instrum. Meth. A **514** (2003) 188.

[5] M. Swartz, et al., Nucl. Instrum. Meth. A **565** (2006) 212.